Integral cross sections and rate constants for the reaction OH+H2→H2O+H: A semiclassical wave packet approach

N. Balakrishnan and G. D. Billing

Citation: The Journal of Chemical Physics **101**, 2785 (1994); doi: 10.1063/1.468469
View online: http://dx.doi.org/10.1063/1.468469
View Table of Contents: http://scitation.aip.org/content/aip/journal/jcp/101/4?ver=pdfcov
Published by the AIP Publishing

Integral cross sections and rate constants for the reaction $OH+H_2 \rightarrow H_2O+H$: A semiclassical wave packet approach

N. Balakrishnan and G. D. Billing
Department of Chemistry, H. C. Ørsted Institute, University of Copenhagen, DK 2100 Ø Copenhagen, Denmark

(Received 30 March 1994; accepted 27 April 1994)

A semiclassical wavepacket method has been introduced to study diatom–diatom exchange reactions of the type $AB+CD \rightarrow ABC+D$; $ABD+C$ using purely inelastic coordinates. The vibrations of the two reagent molecules are treated quantum mechanically by an exact solution of the time-dependent Schrödinger equation. The rotational motions as well as the relative translational motion of the two molecules are treated classically. The coupling between the quantal and classical degrees of freedom is described within an effective Hamiltonian approach. The method has been illustrated for the exothermic reaction $OH+H_2 \rightarrow H_2O+H$ by computing integral cross sections and rate constants. The computed integral cross sections are in reasonable accord with existing quasiclassical trajectory results, but in significant disagreement with recently reported approximate quantum mechanical calculations. The calculated rate constants for the ground vibrational states of the reagents are in good agreement with experimental rate constants in the temperature range $300 \leqslant T \leqslant 700$ K. Comparisons of the rate constants are also made with various theoretical results, including a recently reported six-dimensional quantum mechanical calculation.

I. INTRODUCTION

The significant progress achieved in the theoretical and computational treatments of the quantum reactive scattering process in recent years has resulted in the publication of accurate results for many atom–diatom reactive systems.[1–7] As such calculations are now being reported routinely (though still elaborate), the last couple of years has witnessed a shift in the focus of attention on larger systems, particularly to diatom–diatom reactive scattering.[8–13] The reaction

$$OH+H_2 \rightarrow H_2O+H \qquad \text{(R1)}$$

appears to have become a natural choice for this as most of these studies have focused their attention on it, making it a benchmark system for diatom–diatom reactive scattering calculations. This is quite understandable considering the importance of this reaction in atmospheric as well as combustion chemistry. It is also a main source of water in hydrocarbon-air flames at atmospheric pressure. Furthermore, it has been the subject of several experimental studies which measured rate constants and product state distributions.[14–24]

The presence of three light atoms has made this reaction amenable to accurate *ab initio* calculations. Schatz and Elgersma[25] (SE) had obtained a global potential energy surface (PES) for this system as an analytical fit to the *ab initio* points computed by Walch and Dunning[26] (WD). This PES which we shall refer to as the WDSE PES is considered to be a reasonably good surface for this reaction. Extensive quasiclassical trajectory (QCT) calculations have been carried out by Schatz and co-workers[25,27,28] on this PES. They examined the effect of reagent excitation on the product energy distribution as well as computed integral cross sections and rate constants. Similar studies have been carried out by Rashed and Brown[29] and Harrison and Mayne[30] on their slightly modified versions of the WDSE PES, again using the QCT method. Although these studies have contributed much to the understanding of this reaction, the QCT method has its inherent problem of zero point energy correction which can be exasperating for tetra-atomic system. Reaction (R1) has also been studied in the past employing transition state,[31] variational transition state,[32,33] and quantum-classical reaction path method,[34,35] mostly concentrating on rate constants.

In principle, only a full-dimensional quantum-mechanical calculation can explain all aspects of the dynamics. However, the scope for such calculations is currently very limited, especially from a computational point of view. In a full numerical implementation, the total number of degrees of freedom to be considered is seven compared to four in atom–diatom systems. Due to this, many of the existing time-independent quantum-mechanical methods[1–5] which have scored well for atom–diatom reactive systems will not be computationally viable for tetra-atom reactive scattering processes due to their N^3 scaling property (where N is the number of channels). This has resulted in the development of many approximate reduced dimensionality methods,[8–12] some of which employed rather drastic dynamical constraints. The rotating bond approximation (RBA) of Clary[8] had included three quantal degrees of freedom—the OH rotation, H_2 vibration, and the bending mode in H_2O. He reported integral cross section as well as thermal rate constants. Wang and Bowman[9,10] obtained reaction probability by employing a different RBA method, in which the three bending modes of the tetra-atomic system were treated adiabatically within the harmonic approximation. In a recent study, Echave and Clary[11] have performed planar calculations on this reaction in which the nonreactive OH bond was considered as a spectator. A similar spectator approximation was employed by Zhang and Zhang[12] in a just published five-dimensional (5D) wave packet study of this reaction. To the best of our knowledge, the only published exact quantal calculation on this reaction is the six-dimensional (6D) study

 0021-9606/94/101(4)/2785/8/$6.00

by Manthe *et al.*[13] for zero total angular momentum (J). They computed the cumulative reaction probability for $J=0$, and obtained rate constants in the temperature range 300–700 K within a J-shifting approximation.

Thus, having realized the enormity of the problem in carrying out a full-dimensional quantal calculation, we have pursued an alternative approach based on the semiclassical method. Recent years have seen growing interest in such methods[36–38] as exact quantal calculations are limited to small molecules composed of light atoms. The semiclassical methods retain the simplicity of classical mechanics, but attempts to incorporate the essential quantum effects. Furthermore, depending on the level of sophistication required and the computational facility at one's disposal, it is possible to increase the number of quantal degrees of freedom, thereby making the method closer to the exact.

In our approach for the present system, we treat exactly (quantum mechanically) those degrees of freedom where the quantal effects are most important, whereas the remaining degrees of freedom are treated classically. In the present work, the vibrational motions of the two molecules are treated quantum mechanically using the time-dependent wave packet method. The rotational motions as well as the relative translational motion of the two molecules are treated classically. The coupling between the quantum and classical parts of the system is treated within an effective Hamiltonian approach. In this way, the quantal degrees of freedom is reduced to two compared to seven in a full-dimensional quantal calculation. However, we must reiterate that the present calculations do not make any dynamical constraints or angular momentum decoupling approximations. Higher angular momentum states are included in the calculation in a natural way without invoking any approximations. Thus within the validity of the Hamilton equations of motion for the classical variables, the present calculations should be considered dynamically complete. Another important aspect of our formalism is that only the reagent Jacobi coordinates are employed in the calculation with the products eliminated by employing absorbing boundary conditions.

The rest of this paper is organized as follows: Sec. II provides a description of the coordinate system and the necessary theoretical background. In Sec. III, we introduce the semiclassical effective Hamiltonian, from which are constructed the equations of motion for the classical variables. The wave packet propagation techniques and related computational details are given in Sec. IV. Results of our calculations for the total reaction cross section and rate constants are presented in Sec. V, and a summary of our findings is given in Sec. VI.

II. METHODOLOGY

In the present investigation, we are interested in the study of processes of the type $AB(n_0,j_{01})+CD(m_0,j_{02}) \rightarrow ABC+D$; $ABD+C$ using exclusively the reagent Jacobi coordinates. In the above, n_0 and m_0 are, respectively, the initial vibrational states of the AB and BC molecules, and j_{01} and j_{02} are their corresponding rotational states. The space-fixed coordinate system employed is illustrated in Fig. 1, where $\mathbf{R}_1$ represents the vector joining the atom A to B, $\mathbf{R}_2$ is the vector joining the atom C to D, and $\mathbf{R}_3$ is the vector joining the center of mass of the pairs AB and CD. For the purpose of completeness, we shall derive the full quantum-mechanical Hamiltonian for this collisional system and then introduce the semiclassical approximation used in the actual numerical implementation. The Hamiltonian for this system can be written as follows:

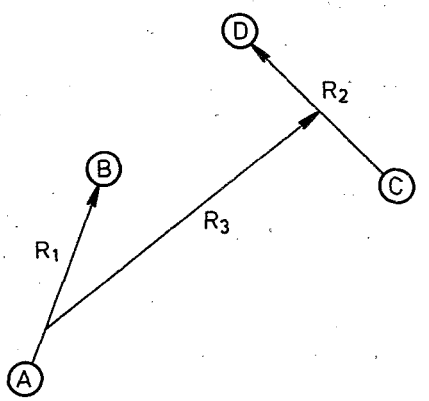

FIG. 1. Reagent Jacobi coordinates.

$$\hat{H}=-\sum_{i=1}^{3}\frac{\hbar^2}{2\mu_i}\left(\frac{\partial^2}{\partial x_i^2}+\frac{\partial^2}{\partial y_i^2}+\frac{\partial^2}{\partial z_i^2}\right)+V[\{R\}], \tag{1}$$

where x_i, y_i, and z_i, $i=1,3$ are the Cartesian components of the three three-dimensional vectors $\mathbf{R}_i$, $i=1,3$, and $\{R\}$ collectively represents the six interatomic distances which define the potential. μ_i, $i=1,3$ are the reduced masses of the AB molecule, CD molecule, and the relative motion of the center of mass of AB with respect to that of CD, i.e.,

$$\mu_1=\frac{m_A m_B}{m_A+m_B}, \tag{2}$$

$$\mu_2=\frac{m_C m_D}{m_C+m_D}, \tag{3}$$

$$\mu_3=\frac{(m_A+m_B)(m_C+m_D)}{M}, \tag{4}$$

where

$$M=m_A+m_B+m_C+m_D. \tag{5}$$

Now we shall introduce three coordinates r_1, r_2, and r_3, which are related to R_1, R_2, and R_3 through the following mass scaling:

$$r_i=\left(\frac{\mu_i}{\mu}\right)^{1/2}R_i, \quad i=1,3, \tag{6}$$

where we have introduced the reduced mass μ as

$$\mu=(\mu_1\mu_2\mu_3)^{1/3}. \tag{7}$$

Similar relations hold for the components of r_i,

$$r_{iq}=\left(\frac{\mu_i}{\mu}\right)^{1/2} q_i, \quad i=1,3, \tag{8}$$

where $q=x$, y, or z. In terms of the mass scaled coordinates, the Hamiltonian in Eq. (1) can be written as

$$\hat{H}=-\frac{\hbar^2}{2\mu}\sum_{i=1}^{3}\left(\frac{\partial^2}{\partial r_{ix}^2}+\frac{\partial^2}{\partial r_{iy}^2}+\frac{\partial^2}{\partial r_{iz}^2}\right)+V[\{R\}]. \tag{9}$$

The components r_{iq}, $i=1,3$ can be expressed in terms of spherical polar coordinates as follows:

$$r_{ix}=r_i \sin\theta_i \cos\phi_i, \tag{10}$$

$$r_{iy}=r_i \sin\theta_i \sin\phi_i, \tag{11}$$

$$r_{iz}=r_i \cos\theta_i, \tag{12}$$

where θ_i and ϕ_i, $i=1,3$ are the six angles defining the orientation of the space-fixed vectors $\mathbf{r}_1$, $\mathbf{r}_2$, and $\mathbf{r}_3$. Introducing the above definitions for r_{iq}, $q=(x,y,z)$, we obtain the Hamiltonian

$$\hat{H}=-\frac{\hbar^2}{2\mu}\sum_{i=1}^{3}\left[\frac{\partial^2}{\partial r_i^2}+\frac{2}{r_i}\frac{\partial}{\partial r_i}+\frac{1}{r_i^2}\left(\frac{\partial^2}{\partial\theta_i^2}+\cot\theta_i\frac{\partial}{\partial\theta_i}+\frac{1}{\sin^2\theta_i}\frac{\partial^2}{\partial\phi_i^2}\right)\right]+V(r_i,\theta_i,\phi_i). \tag{13}$$

The Schrödinger equation satisfying this Hamiltonian may be written as

$$\hat{H}\Psi=E\Psi. \tag{14}$$

The first derivative terms in r_i appearing in $\hat{H}$ can be eliminated by subjecting it to an appropriate transformation. This is achieved by introducing a new wave function ψ in terms of which Ψ is defined as

$$\Psi=\frac{\psi}{r_1 r_2 r_3}. \tag{15}$$

The wave function ψ satisfies the Schrödinger equation

$$\hat{H}'\psi=E\psi, \tag{16}$$

where the new Hamiltonian $\hat{H}'$ is defined as

$$\hat{H}'=r_1 r_2 r_3 \hat{H}(r_1 r_2 r_3)^{-1} \tag{17}$$

$$=-\frac{\hbar^2}{2\mu}\sum_{i=1}^{3}\left[\frac{\partial^2}{\partial r_i^2}+\frac{1}{r_i^2}\left(\frac{\partial^2}{\partial\theta_i^2}+\cot\theta_i\frac{\partial}{\partial\theta_i}+\frac{1}{\sin^2\theta_i}\frac{\partial^2}{\partial\phi_i^2}\right)\right]+V(r_i,\theta_i,\phi_i). \tag{18}$$

The volume element for the normalization of the wave function ψ is $d\tau=\Pi_{i=1}^{3}\sin\theta_i\, dr_i\, d\theta_i\, d\phi_i$.

III. SEMICLASSICAL EFFECTIVE HAMILTONIAN

As mentioned briefly in the Introduction, in the present semiclassical formalism, the vibrational motions of the two diatoms are treated quantum mechanically and the rest of the variables treated classically. Thus r_1 and r_2 form quantal variables. The semiclassical Hamiltonian is obtained from Eq. (18) by replacing the momentum operators corresponding to those variables which are to be treated as classical variables by their respective classical momenta. This leads to

$$\hat{H}_{sc}=\hat{H}_Q+\frac{p_{r_3}^2}{2\mu}+\sum_{i=1}^{3}\frac{1}{2\mu r_i^2}\left(p_{\theta_i}^2+\frac{1}{\sin^2\theta_i}p_{\phi_i}^2\right)+V(r_i,\theta_i,\phi_i), \tag{19}$$

where $\hat{H}_Q$ is a purely quantal Hamiltonian

$$\hat{H}_Q=-\frac{\hbar^2}{2\mu}\left(\frac{\partial^2}{\partial r_1^2}+\frac{\partial^2}{\partial r_2^2}\right). \tag{20}$$

Now we shall define a semiclassical effective Hamiltonian as the expectation value of $\hat{H}_{sc}$ with the quantal wave function. That is,

$$H_{sc}^{eff}=\frac{\langle\psi|\hat{H}_{sc}|\psi\rangle}{\langle\psi|\psi\rangle}, \tag{21}$$

where the brackets denote integration over the quantal variables r_1 and r_2. Thus we obtain

$$H_{sc}^{eff}=H_Q^{eff}+\frac{p_{r_3}^2}{2\mu}+\sum_{i=1}^{3}\frac{1}{2\mu}\left(p_{\theta_i}^2+\frac{1}{\sin^2\theta_i}p_{\phi_i}^2\right)\left\langle\frac{1}{r_i^2}\right\rangle+V^{eff}(r_3,\theta_i,\phi_i), \tag{22}$$

where

$$H_Q^{eff}=\frac{\langle\psi|\hat{H}_Q|\psi\rangle}{\langle\psi|\psi\rangle}, \tag{23}$$

$$\left\langle\frac{1}{r_i^2}\right\rangle=\frac{\langle\psi|1/r_i^2|\psi\rangle}{\langle\psi|\psi\rangle}, \tag{24}$$

and

$$V^{eff}(r_3,\theta_i,\phi_i)=\frac{\langle\psi|V(r_i,\theta_i,\phi_i)|\psi\rangle}{\langle\psi|\psi\rangle}. \tag{25}$$

In the strict sense, Eq. (24) applies to only r_1 and r_2. For notational simplicity, we included r_3 also in that, though it does not cause any harm. Thus from here onwards, $\langle 1/r_3^2\rangle$ should be identified as $1/r_3^2$. Energy conservation requires that H_{sc}^{eff} should be constant throughout the propagation. Equations of motion for the classical variables are obtained from the effective Hamiltonian defined in Eq. (22). Thus we get

$$\dot{r}_3=\frac{p_{r_3}}{\mu}, \tag{26}$$

$$\dot{p}_{r_3}=\left(p_{\theta_3}^2+\frac{p_{\phi_3}^2}{\sin^2\theta_3}\right)\frac{1}{\mu r_3^3}-\frac{\partial V^{eff}(r_3,\theta_i,\phi_i)}{\partial r_3}, \tag{27}$$

$$\dot{\theta}_i=\frac{p_{\theta_i}}{\mu}\left\langle\frac{1}{r_i^2}\right\rangle, \tag{28}$$

$$\dot{\phi}_i=\frac{p_{\phi_i}}{\mu\sin^2\theta_i}\left\langle\frac{1}{r_i^2}\right\rangle; \tag{29}$$

$$\dot{p}_{\theta_i}=\frac{p_{\phi_i}^2\cos\theta_i}{\mu\sin^3\theta_i}\left\langle\frac{1}{r_i^2}\right\rangle-\frac{\partial V^{\rm eff}(r_3,\theta_i,\phi_i)}{\partial\theta_i}, \tag{30}$$

$$\dot{p}_{\phi_i}=-\frac{\partial V^{\rm eff}(r_3,\theta_i,\phi_i)}{\partial\phi_i}. \tag{31}$$

IV. WAVE PACKET PROPAGATION

The dynamical evolution of the system involves simultaneous propagation of the classical as well as quantal degrees of freedom. The solution to the classical part usually involves propagation of a number of trajectories with randomly chosen initial conditions. In our approach here, the evolution of the quantal subsystem is described using the wave packet dynamics. Thus, corresponding to each classical trajectory, we have a wave packet (or "quantum trajectory") describing the vibrations of the two diatomic molecules whose evolution is governed by the time-dependent Schrödinger equation (TDSE)

$$i\hbar\frac{\partial\psi}{\partial t}=\hat{H}_v\psi, \tag{32}$$

where $\hat{H}_v$ is the vibrational Hamiltonian given by

$$\hat{H}_v=\hat{H}_Q+V(r_1,r_2,t). \tag{33}$$

Here the time dependence of the potential comes through the classical variables.

The PES used is the WDSE surface[25] as most of the existing dynamical studies were carried out on that. The analytical fit for this consists of two-, three-, as well as four-body terms and is considered to be reasonably accurate in the transition state region. The surface has a barrier to the reaction of 0.264 eV and an exoergicity of 0.659 eV. Though the *ab initio* points employed for the fitting were fairly accurate, due to the lack of insufficient sampling in the asymptotic region, the fitted surface has some undesirable features in the OH+H_2 entrance channel—a barrier followed by a well as the two molecules approach each other. Various investigators[29,30] have tried to get rid off this unphysical feature, but some of it produced additional wells or barriers. Recently, Clary[8] had used a different procedure to eliminate these undesirable features as it resulted in artificial scattering resonances. However, in the present investigation, we have used the original surface as a bulk of the existing calculations were reported on it.

The initial wave function is taken as the product of two Morse oscillator wave functions representing the vibrations of the two molecules

$$\psi(r_1,r_2,t=0)=\phi_{n_0}(r_1)\phi_{m_0}(r_2), \tag{34}$$

where n_0 and m_0 are the initial vibrational quantum numbers of OH and H_2 molecules, respectively. Propagation of the wave packet, which involves the solution to the TDSE (32), is carried out using the Lanczos algorithm[39,40] together with the fast Fourier transform (FFT) method[41] to compute the second derivatives of the wave function. A variable order Lanczos scheme has been employed in which the number of Lanczos iterations altered at different time intervals by monitoring the magnitudes of the last few recursion vectors. For a time step of 0.1 fs, five to seven Lanczos iterations were found to be sufficient for the last few recursion vectors to become negligible.

Propagation of the classical part involved integration of Eqs. (26)–(31), which was accomplished using a fifth-order Runge–Kutta method. The time increment used for the integration is the same as for the quantal part. Trajectories were chosen randomly with θ_i in the range $0\leqslant\theta_i\leqslant\pi$ and ϕ_i in the range $0\leqslant\phi_i\leqslant2\pi$, where $i=1,3$. The orbital angular momentum quantum number l is defined through the impact parameter (b) using the relation

$$l+1/2=\frac{\sqrt{2\mu_3 E_{\rm trans}}}{\hbar}b, \tag{35}$$

where $E_{\rm trans}$ is the initial translational energy for the relative motion. The orbital angular momentum for each trajectory was defined according to the above relation. All the trajectories were initiated at a center of mass separation $R_0=6$ Å. We had to begin the trajectories at such a large center of mass separation since only at such a large distance does the interaction potential become negligible. This has resulted in large integration times requiring the wave packets to be propagated for a long time, particularly the ones leading to reaction.

V. RESULTS AND DISCUSSION

In the present investigation, we have performed two sets of calculations—one for the total reaction cross section and the other for the thermal rate constant. These are considered separately below.

A. Total reaction cross section

As we are solving the reactive problem essentially as a nonreactive one, an inelastic analysis is employed to obtain reactive informations. The products have been eliminated by placing an absorbing potential along r_2 in the product channel. A linear imaginary potential of the Neuhauser–Baer[42] type has been employed for this purpose. The inelastically scattered wave packet is projected onto the different nonreactive states, once it has reached large internuclear separation, typically 4–5 Å, sufficient enough for any inelastic transitions to cease. The projection is carried out as follows:

$$P_{n,m}^{\rm NR}=\int\int dr_1\,dr_2\,\psi(r_1,r_2,t)\phi_n(r_1)\phi_m(r_2), \tag{36}$$

where the superscript NR stands for nonreactive. The reaction probability is then obtained by subtracting the sum of the nonreactive probabilities from unity as follows:

$$P_{n_0,m_0}^{R}=1-\sum_{n,m}P_{n,m}^{\rm NR}. \tag{37}$$

This procedure is particularly suitable for the present system as there is no third process such as collision-induced dissociation in operation. Once the reaction probability is known for a given trajectory, the total integral cross section for the reaction can be calculated by the usual formula

TABLE I. Convergence of the reaction cross section at $E_{trans}=0.4$ eV with respect to the number of trajectories as well as grid size.

	$\sigma_{0,0}(a_0^2)$	
N_{traj}	Small grid (16,64)	Big grid (32,81)
100	6.805	7.977
150	7.081	7.302
200	7.142	7.045
250	7.116	7.028
300	7.482	7.075

$$\sigma_{n_0,m_0}=2\pi\int_0^{b_{max}} bP^R_{n_0,m_0}db. \tag{38}$$

The standard Monte Carlo method has been used to evaluate the integral. Trajectories have been chosen randomly within the impact parameter range $0-b_{max}$, and for each energy of the calculation, it was ensured that all trajectories with $b>b_{max}$ were nonreactive.

The reaction cross section computed this way should be converged with respect to the grid size as well as the number of trajectories. This is explicitly illustrated in Table I, where we have given the convergence of the reaction cross section at $E_{trans}=0.4$ eV with respect to the number of trajectories (N_{traj}) on two different grids—the smaller grid (16,64) in (r_1,r_2) has spacings $\Delta r_1=0.1$ Å and $\Delta r_2=0.06$ Å, whereas the corresponding spacings in the bigger grid (32,81) are 0.07 and 0.05 Å, respectively. For both grids, the minimum values of r_1 and r_2 were taken to be 0.35 and 0.15 Å, respectively. It can be seen from Table I that the reaction cross section is nearly converged with about 200 trajectories, and the difference between the final cross sections on the two grids is only marginal, indicating that a further increase in grid size is not necessary. So, in all our subsequent calculations, we chose the bigger grid, i.e., the grid (32,81) in (r_1,r_2).

The reaction cross sections have been computed for two different initial conditions of the reagent molecules—one with both H_2 and OH in their ground vibrational-rotational states and the other with the H_2 molecule excited to $v=1$. A number of calculations have been performed for each of these initial conditions at various relative translational energies of the reagents. Reaction cross sections from these calculations are listed in Table II. The number of trajectories integrated to obtain these cross sections is in the range 250–300/energy. b_{max} for these calculations varied from 1.2 Å for the lowest energy to 2.5 Å for the highest energy listed in Table II. As is evident from Table II, $\sigma_{0,0}$ exhibits typical threshold behavior with a small value near the threshold (0.2 eV), followed by a steep increase with E_{trans}. Also included in Table II are the QCT results of Schatz,[27] the RBA results of Clary,[8] results of a 5D wave packet study by Zhang and Zhang,[12] and a 6D quantal result of Szichman and Baer,[43] which was received as a preprint during the preparation of this paper. At lower energies, the present results for $\sigma_{0,0}$ are slightly higher than those of the QCT and RBA results. The corresponding 5D results[12] are significantly lower compared to all other results reported in Table II. Szichman and Baer have only one cross section value at $E_{trans}=0.3$ eV and is about a factor of 2 lower than the present, but a factor of 2.5 higher than the 5D wave packet results. $\sigma_{0,1}$ exhibits large vibrational enhancements and the present results are in good agreement with the QCT results, except at 0.1 eV, where the QCT result is roughly a factor of 2 higher. Clary's RBA results for this seem to be too high at lower energies compared to all other results presented in Table II with $\sigma_{0,1}$ being a factor of 2 larger than the present at 0.2 eV. However, at higher energies, the agreement between the present, QCT, and the RBA results becomes better. Partly, this may have to do with the zero point energy problem at low energies, which is inherent in QCT studies, but can also occur in RBA type dynamically constrained calculations.[12] It may be mentioned that the present study as well as the QCT calculations used the original WDSE PES, whereas the RBA and the 5D calculations employed the modification by Clary[8] to get rid of the unphysical well. Furthermore, both the RBA and the 5D wave packet methods assumed the OH bond to be a spectator, but the former had additional constraints in the geometry which can be considered rather drastic. Thus the large discrepancy seen between RBA and the 5D wave packet results raises concerns about the validity of the approximations that have been employed in these studies. Though the difference between the present and the QCT results is not very large, the present ones should be considered more accurate as the vibrational degrees of freedoms are fully quantized in our approach. Szichman and Baer[43] had employed a 6D quantal calculation, but the interaction region (where the rearrangements take place) has been treated within a quasibreathing sphere approximation, which they do not consider to be very

TABLE II. Computed integral cross sections for two selected initial conditions for the reagents (see the text) compared with various other theoretical calculations.

	$\sigma_{0,0}(a_0^2)$					$\sigma_{0,1}(a_0^2)$			
E_{trans} (eV)	Present	RBA[a]	5D[b]	QCT[c]	6D[d]	Present	RBA[a]	5D[b]	QCT[c]
0.1						2.787	7.66	3.69	6.04
0.2	0.457	0.316	0.155	0.350		10.02	19.0	5.43	13.63
0.3	4.590	2.95	0.945	3.76	2.46	13.35	14.9		12.59
0.4	7.075		2.03			14.02	15.8		
0.5	8.007	8.05	3.01	6.51		15.72			13.19
1.0	10.57			8.69		19.38			15.0

[a]Results from RBA calculations (Ref. 8).
[b]Results from 5D wave packet calculations (Ref. 12).
[c]Results from QCT calculations (Ref. 27).
[d]Results from 6D quantal calculations (Ref. 43).

reliable.[43] Furthermore, they have used other extrapolation procedures in the final evaluation of the cross section. Thus in the wake of these approximations and the fact that energy dependence of the cross section was not reported, it is very difficult to consider it as a benchmark value. As all the studies listed in Table II involve approximations of different kinds, it is difficult to make any claim regarding the exactness of the results in the absence of any exact quantum mechanical calculation or reliable experimental results.

VI. RATE CONSTANTS

With the cross sections just obtained, it is not possible to compute reliable thermal rate constants as higher rotational states are not included in the calculation. So a completely different set of calculations has been performed solely for the purpose of obtaining rate constants by including higher rotational states. This is done by computing an average cross section for the reaction defined as[44]

$$\langle \sigma_{n_0,m_0}(E_c,T_0)\rangle = \frac{\pi\hbar^6}{8\mu_3(kT_0)^3 I_1 I_2}\int_0^{l_{\max}} dl(2l+1) \times \int_0^{j_{1_{\max}}} dj_1(2j_1+1) \times \int_0^{j_{2_{\max}}} dj_2(2j_2+1)P^R_{n_0,m_0}, \quad (39)$$

where $P^R_{n_0,m_0}$ retains its previous definition. μ_3 is the reduced mass for the relative motion and kT_0 is the thermal energy where the reference temperature T_0 (taken as 300 K) vanishes, while evaluating the rate constant. $l_{\max}$, $j_{1_{\max}}$, and $j_{2_{\max}}$ are the maximum values of l, j_1, and j_2 considered for a given classical total energy E_c, I_1 and I_2 are the moments of inertia of OH and H_2 molecules, respectively. The energy E_c is defined as

$$E_c = E_{\text{trans}} + E_{j_1} + E_{j_2} + E_l, \quad (40)$$

where E_{j_1} and E_{j_2} are, respectively, the rotational energies of OH and H_2 molecules, and E_l is the small contribution from the orbital motion as we are starting the trajectories at a finite center of mass separation. Once the average cross sections are available as a function of energy, the rate constants can be computed using the following expression:[44]

$$k_{n_0,m_0}(T) = \left(\frac{8kT}{\pi\mu_3}\right)\left(\frac{T_0}{T}\right)^3 \int_0^\infty d(\beta E_c)e^{-\beta E_c} \times \langle \sigma_{n_0,m_0}(E_c,T_0)\rangle, \quad (41)$$

where $\beta=(kT)^{-1}$. In the following, we shall briefly discuss the computational strategy involved. For each total energy E of the system, a classical total energy is defined as

$$E_c = E - \epsilon_{n_0} - \epsilon_{m_0}, \quad (42)$$

where ϵ_{n_0} and ϵ_{m_0} are the initial vibrational energies of the two molecules. For each randomly chosen trajectory, this total classical energy is then partitioned into rotational and translational parts as in Eq. (40). $l_{\max}$, $j_{1_{\max}}$, and $j_{2_{\max}}$ were sampled in the range 16–40, 8–12, and 4–6 in that order in the energy range $0.7 \leqslant E \leqslant 1.0$ eV. Average cross sections have been generated at seven different E values in this energy range at an interval of 0.05 eV for accurately evaluating the rate constants. A Monte Carlo procedure has been used to evaluate the integral in Eq. (39). Convergence was generally obtained with about 300 trajectories/energy.

TABLE III. Thermal rate constants as a function of temperature for the ground vibrational states of the reagents. Also included in the table are the VTST results of Isaacson and Truhlar (Ref. 32) for comparison.

	$k_{0,0}$ ($cm^3\ s^{-1}$)	
T (K)	Present	VTST
298	0.735*E*-14	1.04*E*-14
350	0.212*E*-13	
400	0.452*E*-13	0.403*E*-13
450	0.811*E*-13	
500	0.130*E*-12	
550	0.190*E*-12	
600	0.259*E*-12	0.223*E*-12
650	0.336*E*-12	
700	0.418*E*-12	

It has been pointed out by Truhlar[45] that for a proper comparison between theoretical and experimental rate constants, it is necessary to account for the effect of the degeneracy of the electronic state in the computed rate constants. This can be included as a statistical factor in the expression for the rate constants[46] and is only necessary in the event of comparing the computed rate constants with experimental results. This factor, referred to as the *multiple surface coefficient*,[45,46] arises from the degeneracy of the electronic state due to spin–orbit splitting. For the present system, only the lower electronic state of the reagents correlates with the the products $H_2O(^1A')+H(^2A')$. The precise value of this factor depends on the magnitude of the spin–orbit splitting as well as the temperature, and for the system investigated here, it is given by the expression $\kappa=[1+\exp(-\Delta/kT)]^{-1}$, where the spin–orbit splitting Δ is 140 cm^{-1}. This gives a value of 0.66 for κ at 300 K and 0.57 at 700 K. Thus, before comparing with experimental rate constants, the computed rate constants should be multiplied with the appropriate value of this factor. A more detailed discussion of this aspect can be found in Refs. 45 and 46. It may be worth pointing out that many comparisons between computed and experimental rate constants for the present system reported in the literature either did not include this factor or assumed it to be 1/2, just the high temperature limit. This factor naturally arises in transition state theory (TST) and has been included in the rate coefficient calculation by Isaacson and Truhlar[32] using the variational TST (VTST). Thus, it would be instructive to compare our computed rate constants with those of Ref. 32. This is provided in Table III, where we have listed the present computed rate constants weighted by the appropriate value of κ, and those from Ref. 32. At 298 K, the VTST rate is about a factor of 1.4 higher than the present, whereas at 400 and 600 K, there is excellent agreement between the two, despite the totally different nature of the two calculations.

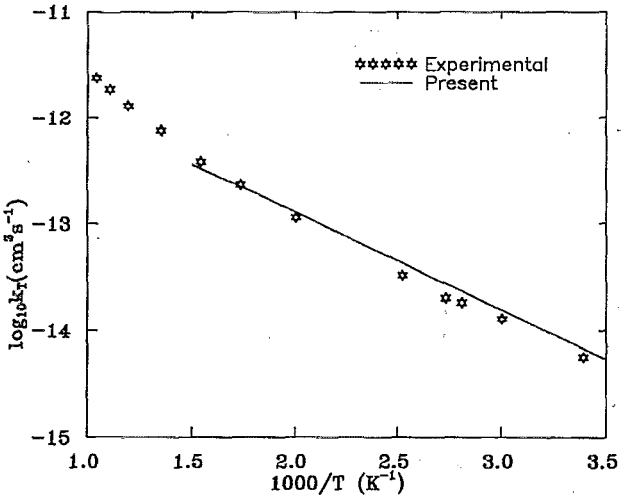

FIG. 2. Arrhenius plots of the computed as well as experimental rate constants (Refs. 14 and 15).

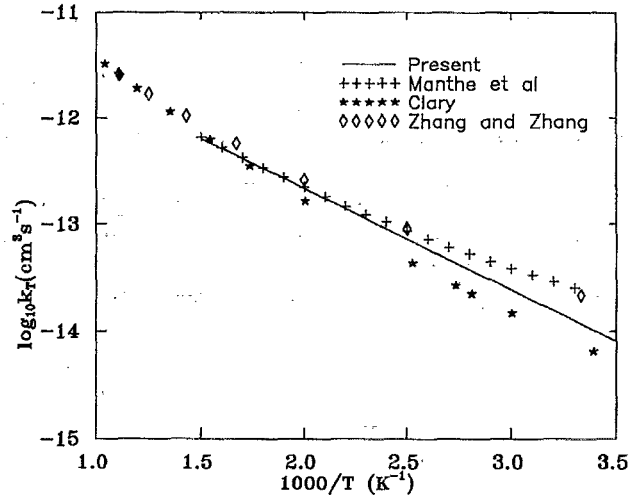

FIG. 3. The same as in Fig. 2, but comparisons are made with other theoretical calculations (see the text).

In Fig. 2, we compare the computed rate constants with the experimental results of Tully and Ravishankara[14] and Ravishankara *et al.*[15] The calculated rate constants are slightly above the experimental ones below 550 K, but cross the experimental values above this temperature. Particularly, the computed rate constant is a factor of 1.2 higher than the experimental one at 295 K, but a factor of 1.15 smaller at 648 K. However, this difference is not significantly higher compared to the experimental error, and the agreement between the two results could be considered near quantitative.

In Fig. 3, we also compare our computed rate constants with various other theoretical results. Included in Fig. 3 are the 6D quantal results of Manthe *et al.*,[13] the 5D wave packet results of Zhang and Zhang,[12] and the RBA results of Clary.[8] As mentioned above, various theoretical results reported in the literature have accounted for the multiple potential energy surface effect in the computed rate constants in different ways. To have a uniform comparison with these theoretical results, we have not included κ in this comparison, and the results of the present calculations shown in Fig. 3 are as obtained from Eq. (41). The results of Zhang and Zhang have been multiplied by 2 as they have assumed this factor to be 1/2 in their rate constant evaluation. Manthe *et al.*'s as well as Clary's results are plotted without any scaling as there was no evidence of inclusion of such a factor in the definition of the rate constant in their papers, nor was it discussed anywhere in the text. It can be seen from Fig. 3 that the present results are in very good agreement with those of Manthe *et al.* at higher temperatures, but the agreement becomes less satisfactory at lower temperatures with the present results being a factor of 2 smaller at 300 K. The results of Zhang and Zhang closely follow those of Manthe *et al.* except at higher temperatures where they are slightly higher. Clary's RBA results are significantly below the present calculated results with the difference being more pronounced at lower temperatures.

The outcome of the above comparison is much against the conclusion of Manthe *et al.* in their communication.[13] They happened to have directly compared their computed rate constants with the experimental results without accounting for the effect of electronic degeneracy. We believe that the large discrepancy observed in their comparison was due to this. Thus their conclusion regarding the quality of the *ab initio* PES is not fully justified unless more elaborate calculations are made available.

VII. SUMMARY AND CONCLUSION

In this paper, we have developed a semiclassical wave packet method to study diatom–diatom exchange reactions within the framework of inelastic scattering. The semiclassical approximation involves treating some degrees of freedom quantum mechanically and the remaining degrees of freedom classically. In the approach described in this paper, the vibrations of the two diatomic molecules are exactly treated by solving the time-dependent Schrödinger equation. The translational and rotational motions of the molecular system are treated classically by defining an effective semiclassical Hamiltonian. The numerical complexity involved in the usual reactive scattering calculations are eschewed in our formalism by employing only reagent Jacobi coordinates. The products have been eliminated by placing an absorbing potential in the product valley, and the reactive information is obtained by performing an inelastic analysis. The method is particularly suitable if detailed state-to-state reactive informations are not required, but only total reaction cross section and rate constants are required. At the same time, due to its very nature, the detailed state-to-state inelastic information is automatically furnished. Another important feature of the method is that the system is treated in its full dimensionality without introducing any dynamical constraints. This is particularly relevant in light of the tremendous numerical effort required for an exact treatment of the dynamics, and the

large discrepancy observed among the various approximate quantal calculations on the system studied in the present investigation.

In the numerical implementation of the present methodology, we have computed the total integral cross section as well as thermal rate constants for reaction (R1). The computed cross sections for $v=0$ and $v=1$ of H_2 are in better agreement with existing QCT results than to approximate quantum-mechanical calculations. Another interesting, but not encouraging observation is that different approximate calculations have produced totally different results. For example, as illustrated in Table II, at $E_{\text{trans}}=0.2$ eV, the RBA cross section of Clary for $v=1$ of H_2 is a factor of 2 larger than the present, whereas the 5D wave packet result of Zhang and Zhang is a factor of 2 smaller. The $v=1$ cross sections are much larger compared to $v=0$ cross sections, particularly at lower E_{trans}, in agreement with other calculations.

The computed rate constants are in good agreement with the experimental rate constants in the temperature range $300 \leqslant T \leqslant 700$ K. Comparisons are also made with various theoretical calculations, which include transition state calculations, and reduced and full-dimensional quantal calculations. The agreement with the VTST results of Isaacson and Truhlar[32] was found to be quite satisfactory. The present results are also in good agreement with the 6D quantal calculation of Manthe *et al.*[13] at higher temperatures, but a factor of 2 smaller at 300 K.

Before we conclude, it may be worth mentioning that compared to exact quantal calculations, the numerical complexity or computational expenses involved in the present calculation are not very large. Furthermore, the results of the present investigation have been quite rewarding, particularly for the rate constants where very good agreement is obtained with the experimental results. Unfortunately, we are unable to make any such claim regarding the reaction cross section as no reliable exact calculation is available for comparison, though agreement with QCT results is generally good. Thus, it is important to perform exact calculations as benchmark studies to assess the validity of various semiclassical and approximate quantal calculations. At the same time, it is equally necessary to develop efficient semiclassical methodologies to study polyatomic reactive scattering at a reasonable computational cost. We believe that the present investigation is an important step towards achieving this goal.

ACKNOWLEDGMENT

This research is supported by the Danish Natural Science Research Council and the Carlsberg Foundation.

[1] G. C. Schatz and A. Kuppermann, J. Chem. Phys. **65**, 4668 (1976).
[2] W. H. Miller, Annu. Rev. Phys. Chem. **41**, 245 (1990); D. E. Manolopoulos and D. C. Clary, Annu. Rep. C, R. Soc. Chem. **86**, 95 (1989).
[3] J. M. Launay and M. Le Dourneuf, Chem. Phys. Lett. **169**, 473 (1990).
[4] J. Z. H. Zhang, Chem. Phys. Lett. **181**, 63 (1991).
[5] (a) A. Kuppermann and P. G. Hipes, J. Chem. Phys. **84**, 5962 (1986); (b) R. T Pack and G. A. Parker, *ibid.* **87**, 3888 (1987); (c) G. C. Schatz, Chem. Phys. Lett. **150**, 92 (1988); (d) J. M. Launay and B. Lepetit, *ibid.* **144**, 346 (1988); (e) S. A. Cuccaro, P. G. Hipes, and A. Kuppermann, *ibid.* **154**, 155 (1989); (f) B. Lepetit and J. M. Launay, J. Chem. Phys. **95**, 5159 (1991).
[6] D. Neuhauser, R. S. Judson, M. Baer, R. L. Jaffe, and D. J. Kouri, Chem. Phys. Lett. **176**, 546 (1991).
[7] N. Marković and G. D. Billing, J. Chem. Phys. **100**, 1085 (1994).
[8] D. C. Clary, J. Chem. Phys. **95**, 7298 (1991); **96**, 3656 (1992).
[9] J. M. Bowman and D. Wang, J. Chem. Phys. **96**, 7852 (1992).
[10] D. Wang and J. M. Bowman, J. Chem. Phys. **98**, 6235 (1993).
[11] J. Echave and D. C. Clary, J. Chem. Phys. **100**, 402 (1994).
[12] D. H. Zhang and J. Z. H. Zhang, J. Chem. Phys. **99**, 5615 (1993); **100**, 2697 (1994).
[13] U. Manthe, T. Seideman, and W. H. Miller, J. Chem. Phys. **99**, 10078 (1993).
[14] F. P. Tully and A. R. Ravishankara, J. Phys. Chem. **84**, 3126 (1980).
[15] A. R. Ravishankara, J. M. Nicovich, R. L. Thompson, and F. P. Tully, J. Phys. Chem. **85**, 2498 (1981).
[16] A. A. Westenberg and N. de Haas, J. Chem. Phys. **58**, 4061 (1973).
[17] I. W. M. Smith and R. Zellner, J. Chem. Soc. Faraday Trans. 2 **70**, 1045 (1974).
[18] K. Kleinermanns and J. Wolfrum, J. Appl. Phys. B **34**, 5 (1984).
[19] A. Sinha, M. C. Hsiao, and F. F. Crim, J. Chem. Phys. **92**, 6333 (1990); **94**, 4928 (1991).
[20] A. Sinha, J. Phys. Chem. **94**, 4391 (1990).
[21] M. C. Hsiao, A. Sinha, and F. F. Crim, J. Phys. Chem. **95**, 8263 (1991).
[22] K. Kessler and K. Kleinermanns, Chem. Phys. Lett. **190**, 145 (1992).
[23] M. J. Bronikowski, W. R. Simpson, B. Girard, and R. N. Zare, J. Chem. Phys. **95**, 8647 (1991).
[24] D. E. Adelman, S. V. Filseth, and R. N. Zare, J. Chem. Phys. **98**, 4636 (1993).
[25] G. C. Schatz and H. Elgersma, Chem. Phys. Lett. **73**, 21 (1980).
[26] S. P. Walch and T. H. Dunning, J. Chem. Phys. **72**, 1303 (1980).
[27] G. C. Schatz, J. Chem. Phys. **74**, 1133 (1981).
[28] G. C. Schatz, M. C. Colton, and J. L. Grant, J. Phys. Chem. **88**, 2971 (1984).
[29] O. Rashed and N. J. Brown, J. Chem. Phys. **82**, 5506 (1985).
[30] J. A. Harrison and H. R. Mayne, J. Chem. Phys. **88**, 7424 (1988).
[31] G. C. Schatz and S. P. Walch, J. Chem. Phys. **72**, 776 (1980).
[32] A. D. Isaacson and D. G. Truhlar, J. Chem. Phys. **76**, 1380 (1982).
[33] D. G. Truhlar and A. D. Isaacson, J. Chem. Phys. **77**, 3516 (1982); D. Lu and D. G. Truhlar, *ibid.* **99**, 2723 (1993).
[34] G. D. Billing, Chem. Phys. **146**, 63 (1990).
[35] G. D. Billing, Chem. Phys. **161**, 245 (1992).
[36] J. T. Muckerman, R. D. Gilbert, and G. D. Billing, J. Chem. Phys. **88**, 4779 (1988).
[37] G. D. Billing and J. T. Muckerman, J. Chem. Phys. **91**, 6830 (1989).
[38] N. Marković and G. D. Billing, J. Chem. Phys. **97**, 8201 (1992).
[39] C. Lanczos, J. Res. Natl. Bur. Stand. **45**, 225 (1950).
[40] T. J. Park and J. C. Light, J. Chem. Phys. **85**, 5870 (1986).
[41] R. Kosloff, J. Phys. Chem. **92**, 2087 (1988).
[42] D. Neuhauser and M. Baer, J. Chem. Phys. **90**, 4351 (1989).
[43] H. Szichman and M. Baer (preprint).
[44] G. D. Billing, Comput. Phys. Commun. **44**, 121 (1987).
[45] D. G. Truhlar, J. Chem. Phys. **56**, 3189 (1972); **61**, 440 (1974).
[46] J. T. Muckerman and M. D. Newton, J. Chem. Phys. **56**, 3191 (1972).